NUMERICAL SIMULATION OF TWO-DIMENSIONAL BUOYANCY-DRIVEN TURBULENCE IN A TALL RECTANGULAR CAVITY*

M. FARHANGNIA, S. BIRINGEN AND L. J. PELTIER†

Department of Aerospace Engineering Sciences, University of Colorado, Boulder, CO 80309, U.S.A.

SUMMARY

A computational study of natural convection of air in a tall rectangular cavity with 4:1 aspect ratio is conducted. In an effort to investigate the applicability of the Boussinesq approximation to turbulent flow simulation, the cavity is differentially heated from the sides and is insulated at the ends at a Rayleigh number of 10^9. Starting from quiescent and isothermal flow conditions, the flow is driven to turbulence without any artificial perturbations. The computer programme developed integrates the two-dimensional, time-dependent Navier–Stokes equations with the Boussinesq approximation and the energy equation by a time-accurate method on a stretched, staggered grid. The simulation proceeds to a statistically steady solution in which large-scale structures are found in the mean. Both mean and fluctuating quantities provide good agreement with experimental results.

KEY WORDS: simulation; turbulence; buoyancy; cavity

1. INTRODUCTION

Buoyancy-driven flows in enclosures have been the subject of extensive numerical and experimental investigations owing to applications in heat transfer engineering. Some of these applications include nuclear insulation, radioactive waste containers and energy storage devices such as solar collectors and double windows and other air gaps in unventilated spaces. Comprehensive reviews[1-3] summarize the main characteristics of buoyancy-driven flows. Accordingly, one area where a lack of understanding still exists is flow behaviour in the high-Rayleigh-number, Ra, turbulent regime which is the focus of the present work.

Flow in a differentially heated cavity is established when fluid near the active vertical walls is convected away by buoyant forces due to a change in density. Since the cavity is enclosed at the ends, a circulatory flow is established. As the fluid travels along the active walls, it passes through several stages. In the entering corner (bottom of the hot wall and top of the cold wall; Figure 1) the flow is initially laminar. It soon passes through a transition region and becomes fully turbulent well before

---

Received 6 May 1994
Revised 21 November 1995

$$\frac{\partial T}{\partial y} = 0$$

$$u = v = 0$$

$y = A$

T_h

$u = v = 0$

T_c

$u = v = 0$

y

x

0 $x = 1$

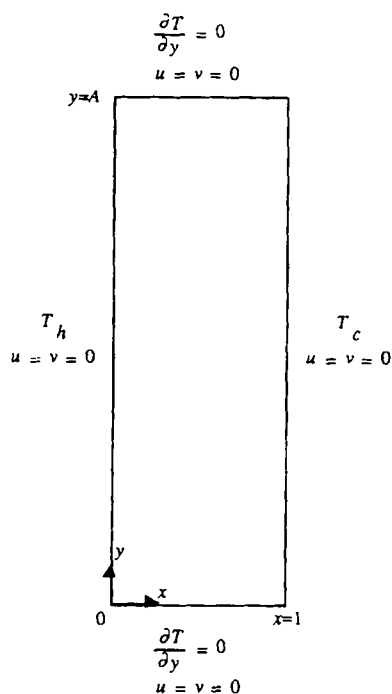$$\frac{\partial T}{\partial y} = 0$$

$$u = v = 0$$

Figure 1. Geometry of cavity considered

the mid-height of the cavity. Once a statistically steady flow is established, the core of the cavity can be roughly characterized as a stably stratified, quiescent flow.

This configuration also provides valuable information for turbulent natural convection along an isolated heated vertical plate in the presence of a stably stratified fluid, as initially noted by Elder.[4] After a measuring velocity and temperature in an enclosed cavity, Elder[4] concluded that the wall layers are similar in behaviour to those of an isolated vertical flat plate. Other investigations of high-Ra flow in an enclosed cavity include those of Kutateladze et al.,[5] who measured heat transfer, velocity and temperature means and their fluctuations, Cowan et al.,[6] who obtained heat transfer data for various aspect ratios, and Giel and Schmidt,[7] who measured velocity and temperature means, their fluctuations, as well as frequency spectra of temperature fluctuations. Paolucci[8] conducted a thorough numerical investigation of turbulent natural convection in a square cavity, obtaining heat transfer data, velocity and temperature means, their fluctuations, as well as probability distributions of fluctuating quantities.

The main emphasis of the present study is to investigate the applicability of the Boussinesq approximations to simulations of turbulent flows. Paolucci[8] suggested that the Boussinesq approximations lead to an inherent symmetry in the flow and cannot accurately simulate buoyancy-driven turbulence without perturbing the flow, making the simulation of the transient state starting from quiescent and isothermal conditions unfeasible. Contrary to what is stated by Paolucci, however, this investigation is able to obtain fully turbulent flow while taking advantage of the Boussinesq approximation, without any artificial perturbations imposed on the flow field.

2. NUMERICAL MODEL

2.1. Governing equations and boundary conditions

An incompressible fluid is considered inside a tall two-dimensional rectangular cavity as shown in Figure 1. The left and right walls of the cavity are isothermal, while the top and bottom are insulated. The left wall is heated to a temperature T_h and the right wall is cooled to T_c. No-slip boundary conditions are imposed on all four sides of the cavity. The flow is initially completely quiescent and isothermal at a temperature $T_0 = \frac{1}{2}(T_h + T_c)$. The gravity vector is in the negative y-direction, perpendicular to the imposed thermal gradient. The aspect ratio A of the cavity is defined to the height of the cavity divided by the width, L_y/L_x.

The mathematical equations governing this fluid are the incompressible Navier–Stokes equations along with the thermal energy equation. In non-dimensional form these may be written as

$$\frac{\partial u}{\partial x} + \frac{\partial v}{\partial y} = 0, \tag{1}$$

$$\frac{\partial u}{\partial t} + \frac{\partial u^2}{\partial x} + \frac{\partial uv}{\partial y} = -\frac{\partial p}{\partial x} + Pr\left(\frac{\partial^2 u}{\partial x^2} + \frac{\partial^2 u}{\partial y^2}\right), \tag{2}$$

$$\frac{\partial v}{\partial t} + \frac{\partial uv}{\partial x} + \frac{\partial v^2}{\partial y} = -\frac{\partial p}{\partial y} + Pr\left(\frac{\partial^2 v}{\partial x^2} + \frac{\partial^2 v}{\partial y^2}\right) - RaPr\beta\Delta T\theta, \tag{3}$$

$$\frac{\partial \theta}{\partial t} + \frac{\partial \theta u}{\partial x} + \frac{\partial \theta v}{\partial y} = \frac{\partial^2 \theta}{\partial x^2} + \frac{\partial^2 \theta}{\partial y^2}, \tag{4}$$

where u, v, θ, p and g are the non-dimensional horizontal velocity, vertical velocity, temperature, pressure and gravitational acceleration respectively. These quantities are non-dimensionalized based on the cavity width L_x, the side wall temperature difference $\Delta T = T_h - T_c$ and the thermal diffusion time scale κ/L_x^2. The non-dimensional temperature θ is defined as $(T - T_0)/\Delta T$. The governing equations include the incompressible Boussinesq approximations, which imply that the fluid properties β and v are constants and that the buoyancy term appears only in the momentum equation as a linear function of the temperature.

The independent non-dimensional numbers that describe buoyant flow in a cavity are the Rayleigh number Ra, which reflects the buoyant contribution, the Prandtl number Pr, which is the ratio of viscous to thermal diffusion, and the aspect ratio A. These quantities are defined as

$$Ra = \frac{\beta\Delta TgL_x^3}{\kappa v}, \qquad Pr = \frac{v}{\kappa}, \qquad A = \frac{L_y}{L_x}. \tag{5}$$

The thermophysical properties used above are the kinematic viscosity v, the thermal diffusivity κ and the coefficient of thermal expansion β. In the present work these parameters are set to $Ra = 10^9, Pr = 0.71$ and $A = 4$, with air as the working fluid.

2.2. Solution procedure and code validation

The governing equations (1)–(4) are solved numerically by a computer code developed by Peltier.[9] The semi-implicit solution procedure employs the Adams–Bashforth explicit method on the convective terms and the implicit Crank–Nicolson method on the viscous terms. Central finite differences are used on a stretched, staggered grid with weighted differences accounting for the

stretching. The momentum equations are discretized by a time-stepping method with second-order accuracy in both time and space. With temporal discretization the momentum equations can be rewritten in index notation as

$$\frac{u_i^{n+1} - u_i^n}{\Delta t} = -\frac{3}{2}\frac{\partial(u_i u_j)^n}{\partial x_i} + \frac{1}{2}\frac{\partial(u_i u_j)^{n-1}}{\partial x_i} - \frac{\partial p^{n+1/2}}{\partial x_i} + \frac{Pr}{2}\left(\frac{\partial^2 u_i^{n+1}}{\partial x_j^2} + \frac{\partial^2 u_i^n}{\partial x_j^2}\right). \tag{6}$$

The time-splitting technique[10,11] is now applied to (6). In the first step of this two-step time advancement method the pressure term is omitted and the equations are discretized at a fractional step (denoted by a 'hat'):

$$\frac{\hat{u}_i - u_i^n}{\Delta t} = -\frac{3}{2}\frac{\partial(u_i u_j)^n}{\partial x_i} + \frac{1}{2}\frac{\partial(u_i u_j)^{n-1}}{\partial x_i} + \frac{Pr}{2}\left(\frac{\partial^2 \hat{u}_i}{\partial x_j^2} + \frac{\partial^2 u_i^n}{\partial x_j^2}\right). \tag{7}$$

Subtracting (7) from (6), one obtains

$$\frac{u_i^{n+1} - \hat{u}}{\Delta t} = -\frac{\partial p^{n+1/2}}{\partial x_i} + \frac{Pr}{2}\left(\frac{\partial^2 u_i^{n+1}}{\partial x_j^2} - \frac{\partial^2 \hat{u}}{\partial x_j^2}\right) \tag{8}$$

$$= -\frac{\partial \phi^{n+1}}{\partial x_i}, \tag{9}$$

where ϕ is a pressure-like scalar quantity to be determined. Taking the divergence of (9) and imposing (equation (1)) at time level $n+1$, a Poisson equation for ϕ is obtained:

$$\nabla^2 \phi^{n+1} = \frac{1}{\Delta t}\frac{\partial \hat{u}}{\partial x_i}. \tag{10}$$

Once ϕ_i^{n+1} is obtained from (10), u_i^{n+1} can be easily calculated from (9) to advance the solution in time. This solution procedure satisfies continuity to machine zero. The Helmholz equations for the momentum and energy and the pressure Poisson equation are solved using the tensor product (eigenvalue decomposition) technique. Further details of this solution procedure can be found elsewhere.[9-12]

The accuracy of the numerical calculation has been established by Peltier and Biringen[13] by comparing solutions with previously published results. Tables I and II compare solutions of the thermally driven cavity with the benchmark calculations of de Vahl Davis,[14] Biringen and Danabasoglu[11] and Le Quere and Penot.[15] Excellent agreement is found in these comparisons, thus verifying the accuracy of the solution technique. Further validation of this solution procedure may be found in Reference 9.

2.3. Resolution requirements

The main difficulties associated with the direct simulation of turbulent flows are the necessity to resolve a wide range of length scales existing in the flow and the inherent three-dimensionality of turbulence.[16,17] The range of length scales grows rapidly with the Reynolds number Re, making many

Table I. Comparison of maximum streamfunction in a thermally driven cavity ($A = 1, Pr = 0.71, Ra = 10^5$)

Current work	de Vahl Davis[14]	Biringen and Danabasoglu[11]
9.58	9.612	9.78

Table II. Comparison of critical Rayleigh number Ra_c and period of oscillation, Π, times square root of Ra in a thermally driven cavity ($A = 4, Pr = 0.71$)

	Current work	Le Quere and Penot[15]
Ra_c	1.7×10^6–1.8×10^6	1.5×10^6–1.7×10^6
$\Pi Ra^{1/2}$	4.97	4.93

interesting fluid dynamics problems unfeasible for direct numerical simulations. To simulate the flow accurately, the grid resolution must be smaller than the smallest existing length scale in the flow.[15] In natural convection, however, the flow is driven by buoyant forces rather than inertial forces, resulting in slow-moving, low-Re flow, relaxing some of the grid-spacing restrictions required for high-Re flows. Second, several experiments, including that of Giel and Schmidt,[7] have concluded that the influence of three-dimensionality is minimal if the cavity is sufficiently deep. Thus the two-dimensional study conducted here should give a physically plausible representation of turbulence in buoyancy-driven flows.

In a rectangular cavity, when the Rayleigh number is in the turbulent regime, the boundary layers on the active walls are highly compact, analogous to an isolated heated vertical plate. Therefore, in order to accurately simulate this flow, the conductive sublayer must be adequately resolved. George and Capp[18] show that for an isolated heated vertical plate the thickness of the conductive sublayer, λ, can be approximated by

$$\lambda \approx 1.7(Pr\ Ra_m)^{-1/3}, \tag{11}$$

where Ra_m is the Rayleigh number based on $\Delta T_m = T_p - T_\infty$ and T_p is the temperature of the plate. For an enclosure, as is the case here, T_∞ is approximated by T_0, making $Ra_m = Ra/2$. Cheesewright[19] offers another estimation for the conductive sublayer,

$$\lambda \approx 3.91 Pr^{1/6} \left(\frac{Ra}{2}\right)^{-1/3}. \tag{12}$$

Using $Pr = 0.71$ and $Ra = 10^9$, the thickness of the conductive sublayer is approximately $2.40 \times 10^{-3} < \lambda < 4.65 \times 10^{-3}$. In the present work, regardless of which approximation we choose, the conductive sublayer is well-resolved with five or six grid points.

As a guideline to ensure the resolution of the smallest flow structures in turbulent natural convection, i.e. the Kolmogorov length and time scales, Paolucci[8] proposed the spatial and temporal spacing requirements

$$\Delta \leqslant \pi(16Pr/Ra)^{3/8}, \tag{13a}$$

$$\Delta t \leqslant 8\pi(Ra^3 Pr)^{-1/4}, \tag{13b}$$

where the mean grid size is defined as $\Delta = (\Delta x \Delta y)^{1/2}$. Quantifying these results for $Pr = 0.71$ and $Ra = 10^9$, one obtains $\Delta \leqslant 3.29 \times 10^{-3}$ and $\Delta t \leqslant 4.86 \times 10^{-6}$.

Throughout this simulation a 121×241 grid is used; Chebychev (cosine) streching is implemented in the vertical and horizontal directions in order to resolve the steep gradients in the vicinity of the walls, satisfying the above requirements. The mean grid size is in the range $1.71 \times 10^{-4} \leqslant \Delta \leqslant 1.85 \times 10^{-2}$, the minimum occurring in the corners of the cavity and the maximum at the centre of the cavity. Thus, except near the centre of the cavity, the smallest scales should be well-resolved.

The time step $\Delta t = 1.25 \times 10^{-7}$ used in the present simulation is well within the guidelines prescribed by (13). Commencing from quiescence, over 3.2×10^5 time steps are computed throughout the simulation, reaching a total non-dimensional time of $t = 4 \times 10^{-2}$, which roughly corresponds to 40 revolution of a particle moving around the cavity with the maximum velocity obtained in the calculations. The mean flow was calculated by sampling the entire flow field over 2.4×10^4 samples for $3.21 \times 10^{-2} \leqslant t \leqslant 4.0 \times 10^{-2}$.

3. RESULTS

In this section, results of the simulation are presented and comparisons are made with previous numerical and experimental investigations. Some of the experimental studies involve isolated heated vertical plates immersed in isothermal or stably stratified fluids. As discussed earlier, such results are useful in analysing the flow inside the boundary layers of the cavity, because these boundary layers are highly compact for Ra as large as 10^9.

3.1. Transient to statistically steady flow

Plate 1 displays isotherms and velocity vectors at several instances in the simulation. As apparent in Plate 1(a), heat is initially conducted from the active side walls, resulting in heated and cooled wall layers which grow in time. The boundary layer is unstable and infinitesimal disturbances near the bottom of the hot wall and the top of the cold wall grow in amplitude (Plates 1(a) and 1(b)). Wave-like structures form and begin to fold back in 'hook'-like patterns (Plate 1(b)). These 'hook'-like patterns have also been observed by others[4,8] and form owing to the penetration of the waves into the core of the cavity, resulting in a deceleration of the fluid, particularly at the tips. This slowing causes the crest of the waves to fold back, developing the distinctive 'hook'-like patterns. The 'hook'-like structures evolve into two large symmetrical vortices on opposite corners, downstream of the active walls (Plate 1(c)). The distinctive vortical structures seem to be a characteristic of the early transient state.[8] As the flow penetrates further into the core, the symmetry observed earlier is broken (Plate 1(d)).

Towards the end of the transient state (Plate 1(e)) and well within the statistically steady state (Plate 1(f)) the behaviour of the flow is consistent with Elder's experimental observations.[4] Boundary layer structures similar to the 'hook' patterns observed early in the transient state are again apparent. These structures are indicative of a mixing region between the wall layers and the interior. As small vortical structures are convected downstream along the active walls, the fluid is entrained from the core and ejected. Between these intense mixing regions a relatively quiescent, stably stratified fluid is observed.

3.2. Mean flow

The mean flow shown in Figure 2 is computed by ensemble averaging the time-averaged data once the diagonal of the cavity. No qualitative change was observed as a result of this process, as it is only served to double the statistical base of the time averaging.

The streamfunction contours obtained from this averaging process reveal two distance cells along the downstream side of the active walls. The development of these cells is due to the large Ra of the present simulation. At very low Ra a unicellular flow is established, and as Ra is increased, the development of the thermal boundary layers steepens the horizontal thermal gradients in the vicinity of the active walls, convecting the fluid downstream. Since this occurs on both active wall sin opposite directions, a region of low vorticity develops in the core of the cavity, leading to two distinct cells. For Ra in the turbulent regime these vortical structures are highly developed.
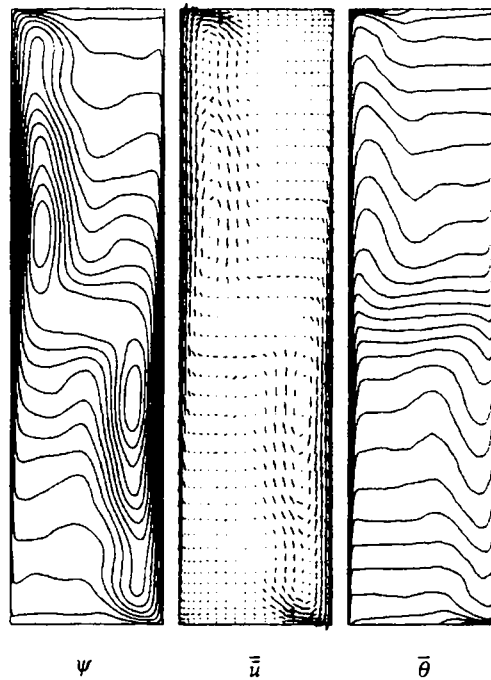
Figure 2. Streamfunction ψ, velocity vectors and isotherms of mean flow

From the mean isotherms, severe isotherm compaction along the active walls can be observed consistent with high-Ra flows.[20] A significant amount of convection is seen to develop near the mid-height of the cavity and the strength of this convection directly determines the strength of the circulation cells revealed in the streamfunction contours. Between these circulation cells the isotherms are characterized by a stably stratified conductive profile in the vertical direction.

In Figure 3 the stratification of the thermal field is nearly linear and the slope is calculated as

$$\beta = A\left(\frac{\partial\bar{\theta}}{y}\right)_{x=1/2} \approx 0.4 \tag{14}$$

in the lower and upper portions of the cavity. This is consistent with Elder,[4] who obtained a slope of 0.35–0.4 in the lower portions of the cavity, and Paolucci[8] and Rutateladze et al.,[5] who obtained similar results across the entire height of the cavity. The slope in the current calculations across the entire height of the cavity is approximated by $\beta \approx 0.6$. The steeper slope near the mid-height of the cavity may be caused by a relatively low Ra of the present calculations. Cowan et al.[6] obtained $\beta = 0.54$ when correlating data for water at various aspect ratios with $1.5 \times 10^7 < Ra < 2.3 \times 10^{11}$, with the lower-$Ra$ calculations corresponding to slightly higher values of β.

3.3. Boundary layer profiles

Profiles of the mean flow at the mid-height of the cavity are studied in this subsection. Since it is the farthest away from the end walls, this particular y-location is chosen in order to obtain a more direct comparison with experimental results of an isolated vertical flat plate, as well as convection flows in enclosures.
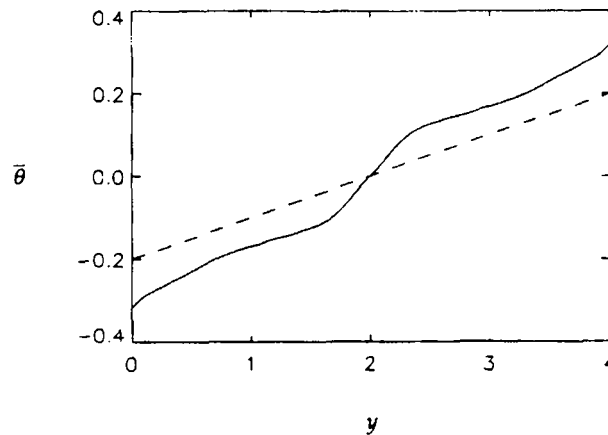
Figure 3. Mean tempeature along mid-width of cavity ($x = 0.5$): ————, present simulation; — — —, straight line of slope 0.4

George and Capp[18] developed a theory for natural convection turbulent boundary layers of heated vertical surfaces. Using classical scaling theory, they showed that the turbulent boundary layer, when fully developed, must be treated in two parts. One is the outer region, consisting of most of the boundary layer, in which viscous and conduction terms are negligible, and the other is the inner region, characterized by a constant heat flux, in which mean convection is negligible. A schematic diagram of these regions is shown in Figure 4.

The inner region consists of two sublayers. Directly next to the wall are the conductive and viscous sublayers, in which both temperature and velocity are linear. The outer part of the inner region is called the buoyant sublayer, where $v \propto x^{1/3}$ while $\theta \propto x^{-1/3}$. The outer region, which contains most
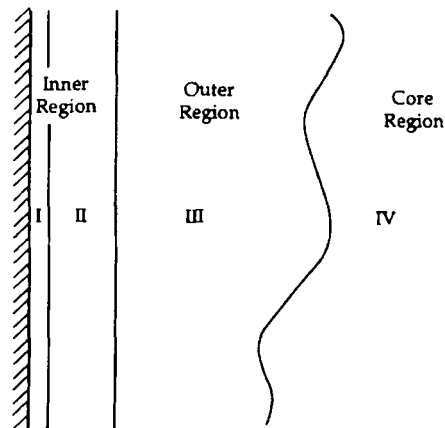
I : Conductive & Viscous Sublayers
II : Buoyant Sublayer
III : Outer (Mixing) Region
IV : Interior/Core Region

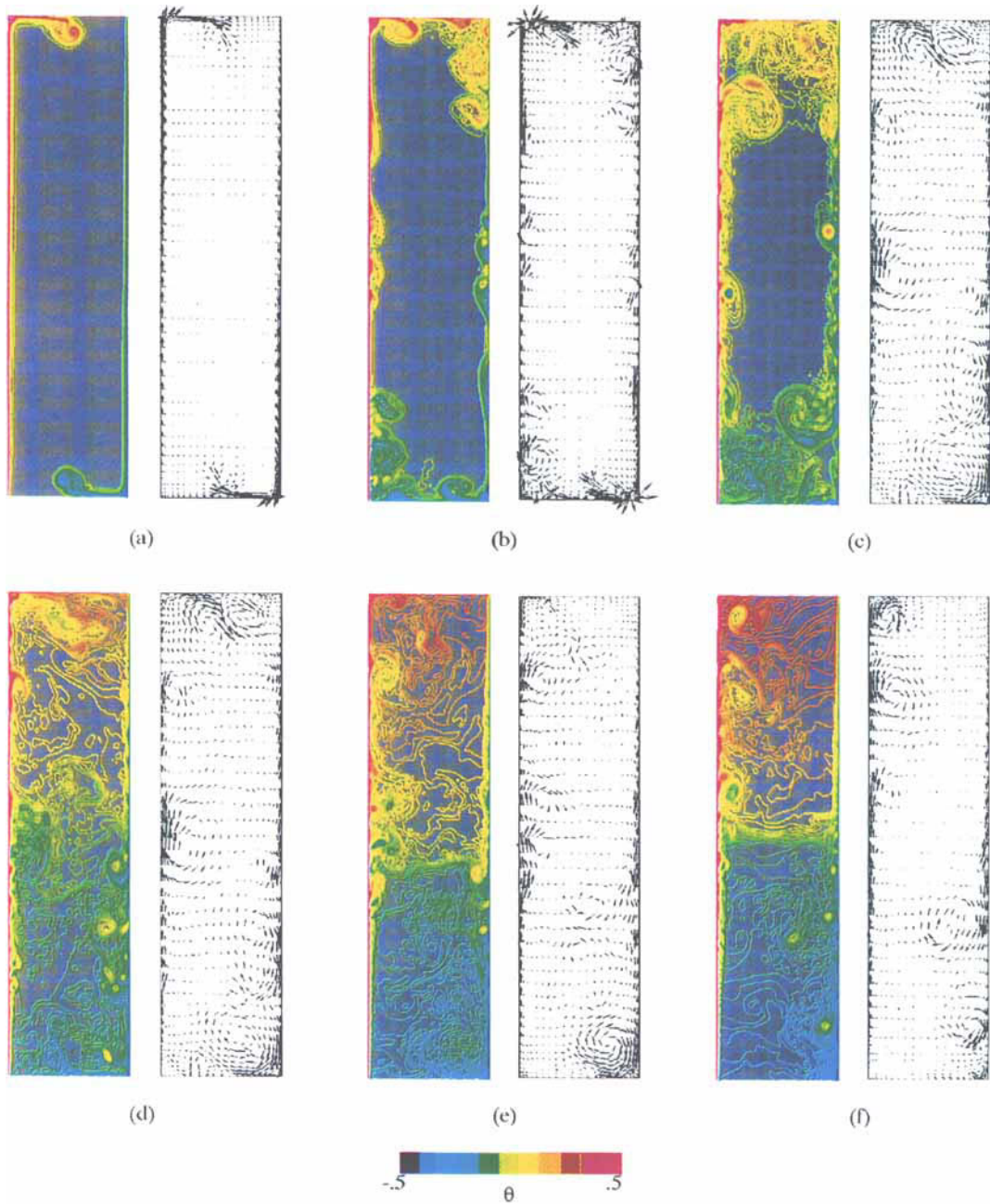Figure 4. Sketch of major regions of boundary layer (adapted from Reference 18)

Plate 1. Isotherms and velocity vectors at various times in the simulation: (a) $t=2\cdot50\times10^{-4}$, (b) $t=5\cdot00\times10^{-4}$, (c) $t=7\cdot50\times10^{-4}$, (d) $t=5\cdot12\times10^{-3}$, (e) $t=1\cdot01\times10^{-2}$ and (f) $t=3\cdot01\times10^{2}$

of the convection in the flow, is found to be self-similar. This is the region Elder[4] refers to as the mixing region in the cavity. These regions developed by George and Capp[18] for heated vertical surfaces are also applicable in the current simulation of an enclosed cavity demonstrating that the turbulent boundary layers are fully developed.

The mean temperature and velocity profiles at the mid-height of the cavity near the hot wall are plotted in Figure 5. The extremely thin thermal boundary layer is clearly evident in Figure (5a). The steep horizontal gradients of both temperature and vertical velocity clearly justify the requirement for the finely stretched grid implemented in the present calculation. The thermal boundary layer extends to $x \approx 0.035$, while the vertical velocity boundary layer extends much further. The convective profile of the vertical velocity depicts the amount of heat transfer in the vertical direction.

Further mean velocity and temperature profiles are shown in Figure 6 for the lower half of the cavity, near the hot wall. From the temperature profiles one can see the stably stratified core near the wall region. The vertical velocity profiles indicate that the maximum velocity is reached before the mid-height of the cavity.
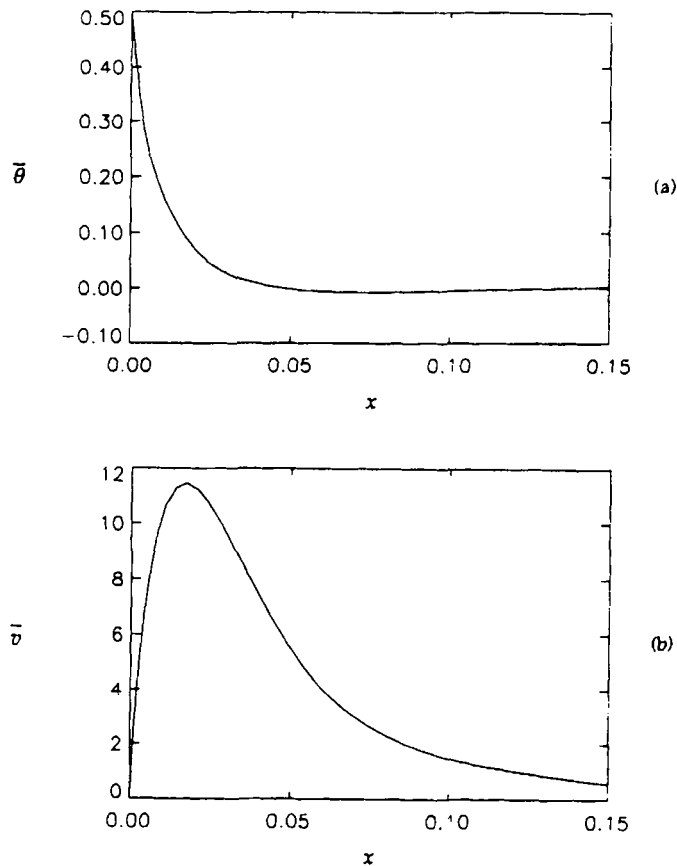

Figure 5. (a) Temperature and (b) vertical velocity profiles at mid-height of cavity ($y = 2$)
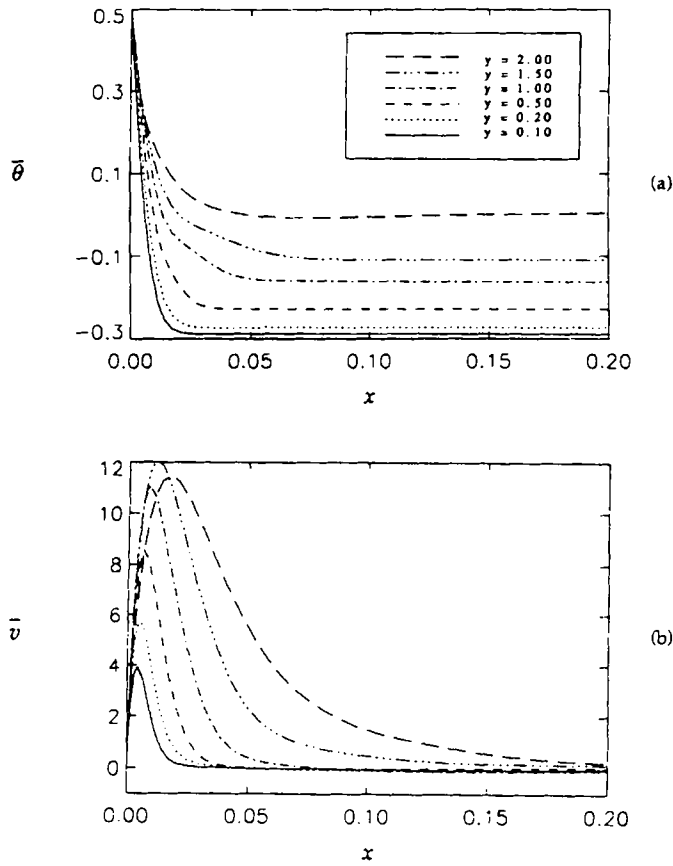
Figure 6. (a) Temperature and (b) vertical velocity profiles at various y-locations near hot wall

To better analyse the inner region of the boundary layer, George and Capp[18] suggest the scaling parameter

$$\eta = \left(\frac{\beta g \Delta T_m L_x^3}{\kappa^2}\right)^{-1/3} = (z\tfrac{1}{2} Ra Pr)^{-1/3} \quad \text{for an enclosed cavity.} \tag{15}$$

To compare results of this investigation with those of George and Capp[18] and Paolucci,[8] the following scales are used for the mean temperature, $\bar{\theta}$, and mean vertical velocity, $\bar{v}$, distributions at the mid-height of the cavity:

$$\phi = 2\bar{\theta}, \qquad V_\eta = \eta \bar{v}. \tag{16}$$

As explained earlier, the conductive sublayer, shown in Figure 7, is characterized by a linear temperature profile. Using the notation of Paolucci,[8] temperature is expressed as

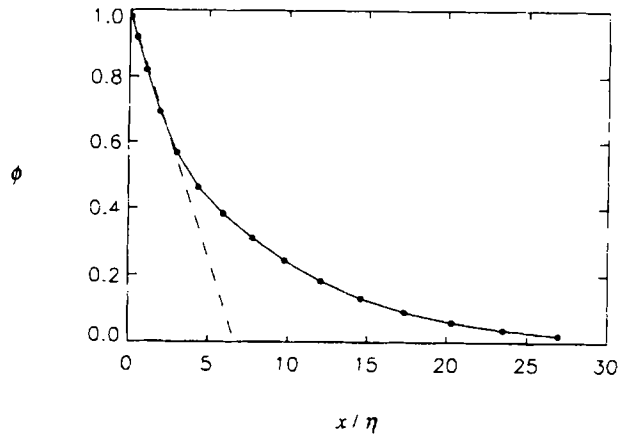$$\phi = 1 - k_1\left(\frac{x}{\eta}\right) \tag{17}$$

Figure 7. Mean temperature profile in conductive sublayer at mid-height of cavity ($y = 2$): ————, present simulation; — -- —, straight line of slope $-k_1$

in the range $0 < x < \lambda$, with $k_1 = 0.14$ and $\lambda = 4.35 \times 10^{-3}$. The thickness of the conductive sublayer is in excellent agreement with that predicted by Cheesewright,[19] $\lambda = 4.65 \times 10^{-3}$. In Table III the slope k_1, as well as other constants $k_2 k_5$ defined later, is compared with the results of Paolucci[8] and George and Capp,[18] showing good agreement.

The conductive sublayer encompasses the viscous sublayer, for which George and Capp[18] obtained an analytical expression for velocity. In terms of variables consistent with the above definitions, this expression can be written as

$$V_\eta = Pr^{-1} \left[k_f \left(\frac{x}{\eta} \right) - \frac{1}{2} \left(\frac{x}{\eta} \right)^2 + \frac{k_1}{6} \left(\frac{x}{\eta} \right)^3 \right],$$

(18)

where k_f is a constant representing the friction coefficient, for which a value of 3.60 is obtained in this study. This compared well with the value obtained by Paolucci,[8] 3.89, differing by only 8%. Using $k_1 = 3.60$, this expression yields a perfect fit for the calculated velocity in the sublayer, confirming its applicability to buoyancy-driven cavity flows.

In Figure 8 and 9 the behaviour of the mean temperature and velocity in the buoyant sublayer is presented. In Figure 8 a linear profile of temperature for $8.4 \times 10^{-3} < x < 2.5 \times 10^{-2}$ is found when plotted against $(x/\eta)^{-1/3}$. This profile can be characterized by

$$\phi = k_2 \left(\frac{x}{\eta} \right)^{-1/3} - k_3,$$

(19)

with $k_2 = 1.94$ and $k_3 = 0.97$ and in good agreement with the Pr dependence obtained by Paolucci,[8]

$$k_2 \approx 2.35 Pr^{1/6},$$

(20)

which yields 2.22 for air. The large difference in k_3 compared with that of George and Capp[18] (Table III) may be attributed to the absence of a stably stratified fluid in their experimental configuration of the heated vertical plate.
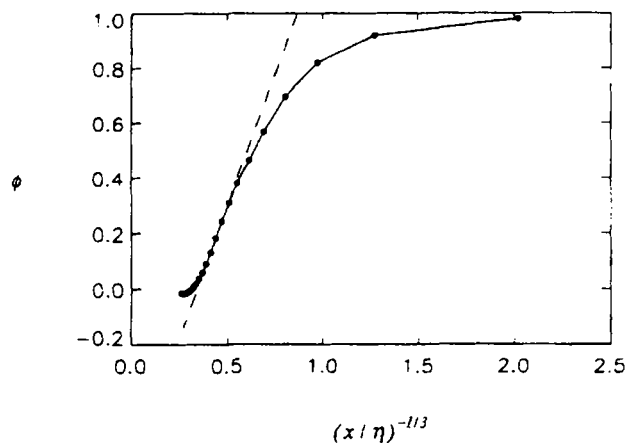
Figure 8. Mean temperature profile in buoyant sublayer at mid-height of cavity $(y = 2)$: ————, present simulation; —·—·—, straight line of slope k_2 and ϕ-intercept k_3
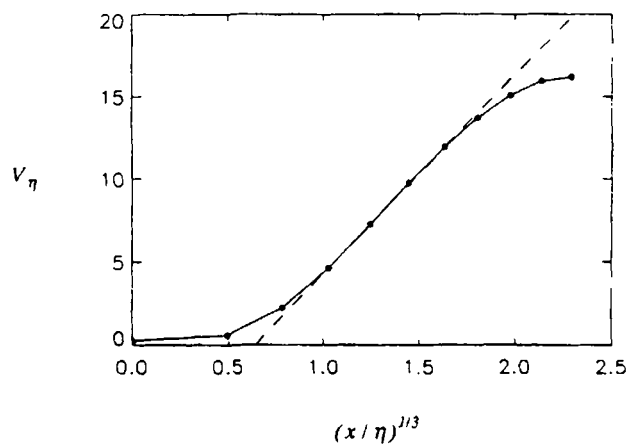

Figure 9. Mean vertical velocity profile in buoyant sublayer at mid-height of cavity $(y = 2)$: ————, present simulation —·—·—, straight line of slope k_4 and V_η-intercept k_5

Table III. Comparison of various constants found in boundary layer calculations in Section 3.3

	k_1	k_2	k_3	k_4	k_5	Description
Enclosed cavity:						
Current work	0·14	1·94	0·97	12·03	7·70	$Pr = 0.71, A = 4$
Paolucci[8]	0·12	2·41	0·94	13·63	8·77	$Pr = 0.71, A = 1$
Vertical plate						
George and Capp[18]	0·1	1·45	0·35	12·3	9·3	$Pr = 0.71$

The linear profile of vertical velocity in the buoyant sublayer is presented in Figure 9, plotted against $(x/\eta)^{1/3}$. Consistent with other studies,[4,18] this relation is valid for a much smaller portion of the sublayer, $1.5 \times 10^{-3} < x < 7.10^{-3}$, relative to that of temperature. The profile of the scaled vertical velocity in this region may be written as

$$V_\eta = k_4 \left(\frac{x}{\eta}\right)^{1/3} - k_5, \tag{21}$$

with $k_4 = 12.03$ and $k_5 = 7.70$. Once again, these results are consistent with those of other studies.

The velocity in the outer regions of the boundary layer is found to be self-similar for an isolated heated vertical surface. By plotting $\bar{v}/V_m$ versus x/δ_v, the vertical velocity collapses to a single profile for fully developed turbulence. Here V_m is the maximum vertical velocity in x and δ_v is the boundary layer thickness defined by

$$\delta_v = \int_0^\infty \frac{\bar{v}}{V_m} dx$$
$$= \int_0^{1/2} \frac{\bar{v}}{V_m} dx \quad \text{for an enclosed cavity.} \tag{22}$$

In Figure 10, using the similarity variables described above, with $V_m = 1.145 \times 10^4$ and $\delta_v = 0.0567$, the present mean vertical velocity profile is compared with that of Paolucci[8] for $Ra = 10^{10}$ and $A = 1$. Although the profiles are quite similar, the collapse to a single profile is not observed. The variance in the profiles may be attributed to the difference in Rayleigh numbers being considered for the two different geometries.

Thus the scaling introduced by George and Capp[18] for isolated heated vertical surfaces in the turbulent regime is also valid for enclosed cavities. As long as a stably stratified fluid is considered outside the boundary layer of the vertical surface, the boundary layers in each geometry exhibit the same characteristics.
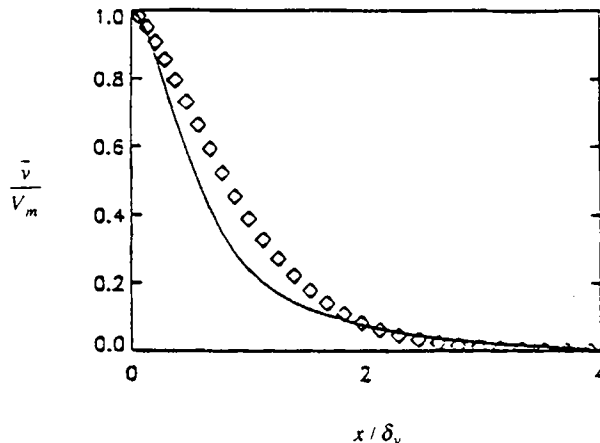

Figure 10. Normalized vertical velocity profile in outer region: ————, present simulation; $\Diamond$, Reference 8

3.4. Correlations and RMS fluctuations

One-point correlations are computed at every grid location in the cavity for $3 \cdot 25 \times 10^{-2} < t < 4 \cdot 0 \times 10^{-2}$ over $1 \cdot 2 \times 10^4$ samples. These results help to quantify the intensity of the turbulence present in the cavity.

Profiles near the hot wall are shown in Figure 11 at the mid-height of the cavity.

The general behaviour of all three quantities, $(\theta'^2)^{1/2}, (\overline{u'^2})^{1/2}$ and $(\overline{v'^2})^{1/2}$, is consistent with experimental results of Kutateladze et al.[5] and Giel and Schmidt,[7] as well as with numerical results of Paolucci.[8] the maxima for temperature and vertical velocity fluctuations occur near the location of the maximum velocity, $x_m = 0 \cdot 017$. The maximum amplitudes reach $0 \cdot 40$ and $0 \cdot 3$ for vertical velocity and temperature fluctuations respectively. These agree remarkably well with the values of $0 \cdot 40$ and $0 \cdot 14$ obtained by Kutateladze et al.[5] The maximum RMS fluctuations of vertical velocity computed by Paolucci[8] are approximately half of those observed in the experimental studies. He attributes the difference to the Pr dependence of the viscous and conductive sublayer thicknesses. The computed values of the present simulation using the same Pr ($0 \cdot 71$) seem to challenge this conclusion.

Another local maximum of $(\overline{v'^2})^{1/2}$ is observed near $x = 0 \cdot - 6$. This local maximum is near the location of maximum horizontal velocity. The occurrence of this second hump is in strong agreement with both experimental results and numerical results of Paolucci.[8] It reflects the continued mixing taking place in the boundary layer and should be considered when developing turbulence models for this type of problem.

3.5. Time dependence

Spectral analysis is used in turbulence investigations as a tool to analyse instantaneous flow characteristics. If only a few distinct frequencies are apparent in the frequency spectra, the flow may be termed somewhat chaotic but not yet turbulent. As the driving force is increased, more and more frequencies become energized. The flow is turbulent when the spectra are marked by broadband components of frequency.

Figure 12 shows a brief time history of the temperature at a fixed point at the mid-height of the cavity in the vicinity of the hot wall. The frequency content of this particular time sample is shown in
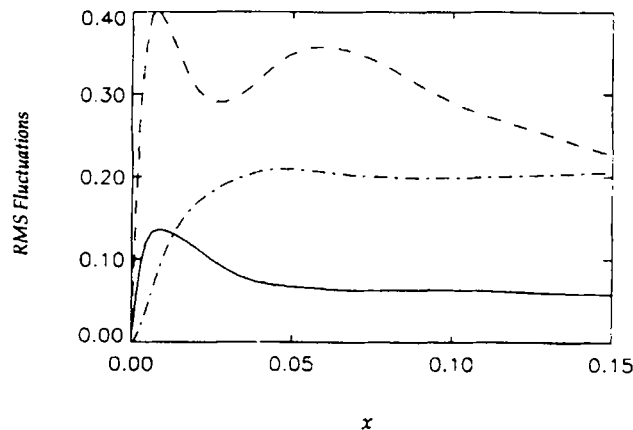

Figure 11. RMS quantities in vicinity of hot wall at mid-height of cavity ($y = 2$): ———, $(\overline{\theta'^2})^{1/2}$; — — ·, $(\overline{v'^2})^{1/2}/V_m$; — · —, $(\overline{u'^2})^{1/2}/V_m$
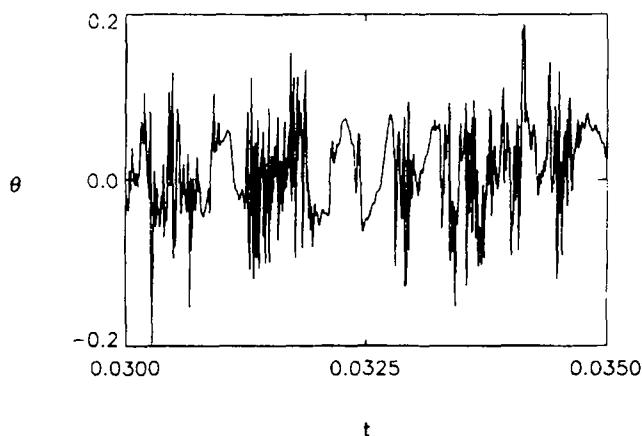
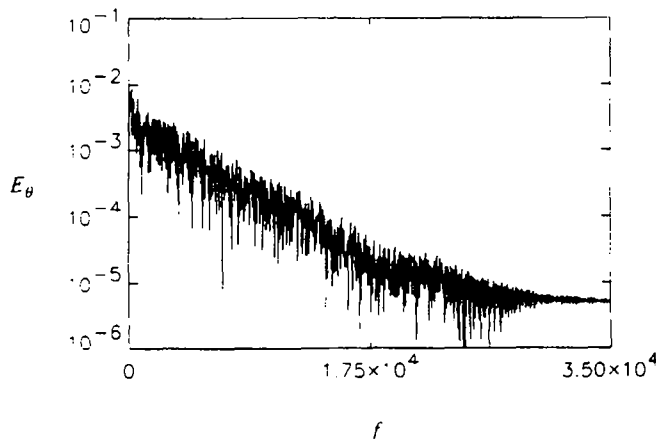Figure 12. Brief time history of temperature at $(x, y) = (0.1, 2.0)$

Figure 13. Frequency spectra of time sample shown in Figure 13

Figure 13. The frequency spectrum has broadband character indicative of fully developed turbulent flow. The frequency range shows good agreement with the results of Paolucci and Chenoweth[21] and Giel and Schmidt.[7]

4. CONCLUSIONS

A numerical simulation of two-dimensional turbulent natural convection has been conducted. Starting from quiescent, isothermal conditions, transient effects are observed using the time-dependent Navier–Stokes equations. Unstable boundary layers are quickly established along the active walls. Infinitesimal disturbances near the entry corners soon grow in amplitude, resulting in distinctive 'hook'-like patterns along the active walls as seen in experimental results. As a statistically steady solution is reached, strong mixing regions are observed between the wall layers and the relatively quiescent, stably stratified core.

The Boussinesq approximation is shown to be valid in buoyancy-driven turbulent flow, enabling the simulation of the full transitional and turbulent flow starting from quiescent initial conditions. Mean and first-order turbulence quantities show excellent agreement with both experimental and numerical results not implementing this assumption; the broadband frequency spectra are also indicative of fully developed turbulent flow. The precise effect of machine round-off and truncation errors, inherently contained in all numerical solutions, is difficult to ascertain and was not attempted in this work.

Time- and ensemble-averaged mean flow reveals two distinct vortex structures along the downstream side of the active walls due to the large Ra of the calculation. From isotherms, strong convection is seen to develop near the mid-height of the cavity and severe isotherm compaction is observed near the active walls. The isotherm compaction allows comparisons to be made with turbulent boundary layer theory along isolated vertical heated surfaces, developed by George and Capp.[18] This theory is also found to be valid for enclosed cavities. The outer region, which contains most of the convection in the flow, is found to be nearly self-similar when compared with the results of Paolucci.[8] RMS fluctuations and frequency spectra indicate fully developed turbulent flow, where fluctuations are found to be more pronounced along the active walls.

REFERENCES

1. S. Ostrach, 'Natural convection in enclosures', *Adv. Heat Transfer*, **8**, 161 91972).
2. S. Ostrach, 'Natural convectin in enclosures', *J. Heat Transfer*, **110**, 1175 (1988).
3. K. Yang, 'Transitions and bifurcations in laminar buoyant flows in confined enclosures, *J. Heat Transfer*, **110**, 1191 (1988).
4. J. Elder, 'Turbulent free convection in a vertical slot', *J. Fluid Mech.*, **23**, 99 (1965).
5. S. Kutateladze, S. Ivakin, V. Kirdyshkin and A. Kerkolov, 'Thermal free convection in a liquid in a vertical slot under turbulent flow conditions', *Heat Transfer Sov. Res.*, **10**, 193 (1978).
6. G. Cowan, P. Lovegrove and G. Quarini, 'Turbulent natural convection heat transfer in vertical single water-filled cavities', in *Heat Transfer 1982*, Washington, Vol. 2, 1982, p. 195.
7. P. Giel and F. Schmidt, 'An experimental study of high Rayleigh natural convection in an enclosure', *Heat Transfer 1986*, Washington, Vol. 4, 1986, p. 1459.
8. S. Paolucci, 'Direct numerical simulation of two-dimensional turbulent natural convection in an enclosed cavity', *J. Fluid Mech.*, **215**, 229 (1990).
9. L. Peltier, 'Numerical simulation of time-dependent convection in layered fluid systems', *Ph.D. Thesis*, University of Colorado, Boulder, CO, 1992.
10. J. Kim and P. Moin, 'Application of a fractional step method to incompressible Navier–Stokes equations', *J. Comput. Phys.*, **59**, 308 (1985).
11. S. Biringen and G. Danabasoglu, 'Oscillatory flow with heat transfer in a square cavity', *Phys. Fluids A*, **1**, 1796 (1989).
12. L. Peltier, S. Biringen and A. Chait, 'Application of implicit numerical techniques to the solution of the three-dimensional diffusion equation', *Numer. Heat Transfer B*, **18**, 205 (1990).
13. L. Peltier and S. Biringen, 'Time-dependent thermocapillary convection in a shallow Cartesian cavity: numerical results for a moderate Prandtl number fluid', *J. Fluid Mech.*, **257**, 339 (1993).
14. G. de Vahl Davis, 'Natural convection in a square cavity: A benchmark numerical solution', *Int. j. numer. methods fluids*, **3**, 249 (1983).
15. P. Le Quere and F. Penot, 'Numerical and experimental investigation of the steady to unsteady natural convection of air in a vertical differentially heated cavity', in *Bifurcation Phenomena in Thermal Processes and Convection*, ASME, NY, 1987, p. 75.
16. G. Grotzbach, 'Spatial resolution requirements for direct numerical simulation of the Rayleigh–Benard convection', *J. Comput. Phys.*, **49**, 241 (1983).
17. H. Tennekes and J. L. Lumley, *A First Course in Turbulence*, MIT Press, Cambridge, MA, 1971.
18. W. George and S. Capp, 'A theory for natural convection turbulent boundary layers next to heated vertical surfaces', *Int. J. Heat Mass Transfer*, **22**, 813 (1979).
19. R. Cheesewright, 'Turbulent natural convection from a vertical plane surface', *J. Heat Transfer*, **90**, 1 (1968).
20. N. Markatos and C. Pericleaous, 'Laminar and turbulent natural convection in an enclosed cavity', in *Natural Convection in Enclosures—1983*, New York, Vol. 26, 1983, p. 59.
21. S. Paolucci and D. Chenoweth, 'Transition in chaos in a differentially heated vertical cavity', *J. Fluid Mech.*, **201**, 379 (1989).